JACS
JOURNAL OF THE AMERICAN CHEMICAL SOCIETY
Article
pubs.acs.org/JACS

The Effect of a Solid Surface on the Segregation and Melting of Salt Hydrates

Yu Zhang, Emmanuel Anim-Danso, and Ali Dhinojwala*

Department of Polymer Science, The University of Akron, Akron, Ohio 44325-3909, United States

Supporting Information

ABSTRACT: Considering the importance of salt and water on earth, the crystallization of salt hydrates next to solid surfaces has important implications in physical and biological sciences. Heterogeneous nucleation is driven by surface interactions, but our understanding of hydrate formation near surfaces is limited. Here, we have studied the hydrate formation of three commonly prevalent salts, $MgCl_2$, $CaCl_2$, and NaCl, next to a sapphire substrate using surface sensitive infrared-visible sum frequency generation (SFG) spectroscopy. SFG spectroscopy can detect the crystallization and melting of salt hydrates at the interface by observing the changes in the intensity and the location of the cocrystallized water hydroxyl peaks (3200−3600 cm^{-1}). The results indicate that the surface crystal structures of these three hydrates are similar to those in the bulk. For the NaCl solution, the brine solution is segregated next to the sapphire substrate after the formation of the ice phase. In contrast, the $MgCl_2$ and $CaCl_2$ surface hydrate crystals are interdispersed with nanometer-size ice crystals. The nanosize ice crystals melt at much lower temperatures than bulk ice crystals. For NaCl and $MgCl_2$ solution, the NaCl hydrates prefer to crystallize next to the sapphire substrate instead of the ice crystals and $MgCl_2$ hydrates.

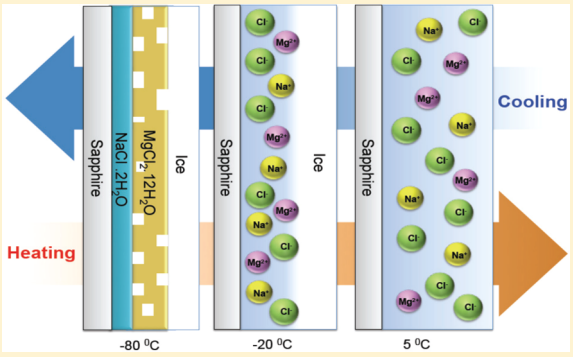

INTRODUCTION

The formation of salt hydrates is of scientific and technological interest in the areas of energy storage,[1,2] biology,[3,4] climatology,[5] and geology.[6−11] The salt hydrates are formed by cooling an aqueous salt solution which leads to phase separation between the salt-rich brine solution and the freezing of water to form ice. Further cooling results in concentrating the brine solution and increasing the thickness of the ice layer, and eventually in the freezing of the salt-hydrates near the eutectic concentration.[12] The number of water molecules cocrystallized in the hydrate crystal depends on the chemistry of the salt. Hydrate formation and its phase diagram have been studied by measuring thermal properties,[1,2,13] X-ray diffraction,[14−17] Raman,[18−20] and infrared spectroscopy.[21−24] In Raman and IR spectroscopy, the observation of sharp absorption bands between 3200 and 3600 cm^{-1} has been used to identify the hydrogen-bonding structure of the hydroxyl groups incorporated in the salt hydrates.

Although our knowledge of the phase diagram of hydrate formation in solutions is well established, direct experiments to observe the formation of salt hydrates near surfaces have not been done. The role of ions and mineral nanoparticles on ice nucleation have been previously reported, and ions tend to lower the nucleation temperature compared to mineral nanoparticles.[25−27] However, the nucleation rates are influenced by the size of the mineral nanoparticles, and the role of surface is still not clear. Studying hydrate formation near solid surfaces could provide a broader understanding of the role of ions and water interactions in controlling heterogeneous nucleation of hydrate crystals next to solid surfaces. Understanding heterogeneous nucleation is also important in controlling the uniformity of crystals, and thus the energy stored and released in phase change materials for energy applications.[1,2,13] The uniformity of hydrate crystals and the segregation of brine next to solid surfaces are also important for ice adhesion and friction, properties which are very relevant in understanding the movement of glaciers formed from seawater[28] and in mitigating ice formation on aircrafts, power lines, and wind turbine blades. One could also imagine that the surface segregation of brine may have played an important role in sustaining life at low temperatures and has important consequences in our understanding the origin of life. In addition to the importance of this problem on earth, where we have an abundance of salt water, it is also becoming increasingly important to understand the role of water on other planetary bodies[6,29] where hydrates are found as inclusions in mineral layers.

We have combined a surface sensitive sum frequency generation (SFG) technique with a novel design of a low temperature heating/cooling sample holder to study the formation of salt hydrates next to a sapphire surface.[30] SFG is a second order nonlinear optical technique that involves mixing a short-pulse high intensity visible laser (ω_{vis}) with a tunable infrared laser (ω_{IR}). Based on the dipole approximation, the SFG signal, at the sum of $\omega_{SFG} = \omega_{vis} + \omega_{IR}$, is only generated at interfaces in systems where the bulk is centrosymmetric. By combining SFG

Received: July 5, 2014
Published: October 1, 2014

   dx.doi.org/10.1021/ja5067866 | J. Am. Chem. Soc. 2014, 136, 14811−14820

with a total internal reflection geometry, this technique offers the ability to study the structure and transition temperature of molecules next to a solid interface. The probe depth in SFG experiments is the distance from the surface to the position where the anisotropic molecular orientation becomes isotropic. Previously, we have demonstrated the use of this approach to monitor the formation of NaCl hydrate.[30] Here, we have studied the freezing and melting of three common salt solutions, $MgCl_2$, $CaCl_2$, and NaCl. These three cations (Mg^{2+}, Ca^{2+}, and Na^+) are abundant in geological and biological systems and are used as phase-change materials for energy storage applications.[1,2] These three salt solutions also have very different eutectic concentrations, transition temperatures, and coordination numbers of water molecules in the bulk hydrate crystals. In addition to measuring the structure formation, we have also measured the differences in surface and bulk transition temperatures for the three salt solutions and a mixture of salts (NaCl and $MgCl_2$) using identical conditions. Surprisingly, in the case of the mixture, the competition between the two ions resulted in the segregation of the NaCl hydrate next to the sapphire substrate.

EXPERIMENTAL SECTION

Sample Preparation. The sapphire prisms and cells were sequentially sonicated for 1 h in different solvents (toluene, acetone, methanol, and deionized water) to remove nonpolar and polar contaminants. After the solvent treatments, the prisms were rinsed by deionized water and dried using a slow stream of nitrogen gas. To further remove any surface organic residues, the final step involved cleaning the sapphire prisms using air plasma for 4 min. The stainless cells were heated in an oven at 120 °C for 1 h and cleaned by air plasma for 2 min before the experiments. Ultrapure water (18.2 MΩ/cm from a Millipore filtration system) was used in these experiments. X-ray photoelectron spectroscopy (XPS) was used to verify that the adventitious hydrocarbons signals were less than 5%, and the SFG spectra of blank sapphire prisms were checked to make sure that there were no spectral features between 2750 and 3000 cm^{-1}, indicating minimal hydrocarbon contamination on the sapphire surface. The salt solutions with different concentrations were prepared using NaCl (purity ≥99%, anhydrous, powder, purchased from Fisher Scientific), $MgCl_2$ (purity ≥98%, anhydrous, powder, purchased from Sigma-Aldrich), or $CaCl_2$ (purity ≥97%, anhydrous, powder, purchased from Sigma-Aldrich). The SFG spectra collected for NaCl baked at 538 °C for 2 h were not affected by this additional heating step. For $MgCl_2$, we used activated carbon for purification, followed by filtration, and this also did not affect the SFG results.

SFG Measurements. The SFG experiments were performed using a picosecond Spectra Physics laser system with a ∼3.5 μJ tunable IR beam (2000−3800 cm^{-1}, 1 ps pulse width, 1 kHz repetition rate, and a diameter of 100−200 μm) and a ∼70 μJ visible beam (800 nm wavelength, 1 ps pulse width, 1 kHz repetition rate, and a diameter of 1 mm).[30,31] The IR beam energy used in this work had a negligible effect on the laser heating of the ice or hydrate. The measured transition temperature of ice into water at the surface occurred at 0 °C.[31] The SFG measurements involved spatial and temporal overlap of the two laser beams on the sample. A motorized, computer-controlled delay stage was used to ensure that the temporal delay was maintained while scanning IR frequencies from 2800 to 3800 cm^{-1}. We have used a total-internal-reflection (TIR) geometry with an equilateral 60° sapphire prism and a 16° incident angle with respect to the surface normal to probe the sapphire−brine and sapphire−hydrate interface.[32,33] The total internal reflection angle depends on the refractive index of brine (critical angle ∼16°) and hydrate (critical angle ca. −2° to ∼10°), and also the refractive index varies as a function of wavelength. However, we have fixed the incident angle in this experiment because of the windows used for the vacuum cell. We estimate that for 2700 cm^{-1}, the SFG intensity will be ∼53% of the value at 4200 cm^{-1} for the water−sapphire system. Nevertheless, the hydrate peaks are relatively sharp and the spectral features will not be affected by the changes in the critical angle as a function of wavenumber. We have estimated the thickness of the brine and salt hydrate layers as follows: For 0.1 M solutions at eutectic temperatures, the thickness is ∼25 μm for $MgCl_2$ brine, ∼7 μm for $MgCl_2$ hydrate, ∼20 μm for $CaCl_2$ brine, ∼12 μm for $CaCl_2$ hydrate, ∼14 μm for NaCl brine, and ∼5 μm for NaCl hydrate. The refractive indices of brine and ice/water are very similar and for the conditions used here, we are primarily probing the sapphire−brine interface. For hydrates, it is possible that for 16° incident angle, we may have SFG signals from both sapphire/hydrate and hydrate/ice interfaces. However, because of absorption/scattering by the thick hydrate layers, we anticipate the SFG signals to be dominated by the sapphire/hydrate interface. The results for NaCl hydrate experiments support this hypothesis because we do not observe ice peaks after the formation of the NaCl hydrate crystals.[30] Because of these reasons, we have assumed that the SFG signals are generated from the sapphire/hydrate interface rather than the hydrate/ice interface. The incident angle of the visible beam was 1−2° lower than that of the IR beam. The SFG signals were collected using a photomultiplier tube connected to a 0.5 m spectrometer. We have collected SFG spectra using both PPP (p-polarized SFG output, p-polarized visible input, and p-polarized IR input) and SSP (s-polarized SFG output, s-polarized visible input, and p-polarized IR input) polarizations. The SSP and PPP polarizations provide complementary information which can be used to provide information on the orientation of molecules at the interface. Because of the similarity in the SSP and PPP spectra for hydrate and brine solutions, for pure hydrates, PPP spectra are shown in the paper, and the SSP spectra are shown in Supporting Information (Figure S1−S2). A Lorentzian fitting function was used to fit all the SFG spectra.[31,33] The peak position provides the chemical identity of the interfacial molecules, and the amplitude strength is proportional to the concentration and the orientation of the interfacial molecules.

$$I_{\mathrm{SFG}} \propto \left| \chi_{\mathrm{eff,NR}} + \sum \frac{A_q}{\omega_{\mathrm{IR}} - \omega_q - i\Gamma_q} \right|^2 \quad (1)$$

where A_q, ω_q, and Γ_q are the amplitude, angular frequency, and damping constant of the qth vibrational resonance. $\chi_{\mathrm{eff,NR}}$ describes the nonresonant contribution.

Heating and Cooling Cell. Water condensation is one of the biggest challenges in low temperature measurements; we have designed a vacuum cell (pressure of 0.13 Torr) to house the sapphire prisms to reduce water condensation. The salt solution was sealed in the inner chamber with a sapphire prism on one side and a customized temperature stage (Instec Inc.) on the other side. A steel dome was designed with CaF_2 windows to allow the passage of the visible and IR input beams and the SFG output beam. The pure hydrate experiments were conducted using a rate of 5 °C/min with 30 min equilibration time every 5 °C change in temperature in cooling, and 0.5 °C/min with 30 min equilibration time every degree change in temperature in heating. For the mixtures of the NaCl and $MgCl_2$, we used a rate of 1 °C/min with 10 min equilibration time between every degree change in temperature in the slow cooling cycle, 0.5 °C/min with 30 min equilibration time every degree change in temperature in the heating cycle, and 5 °C/min with 5 min equilibrium time every 10 °C change in temperature in the fast cooling cycle. The details of the experimental cell were provided in previous publications.[30,31]

Reflectivity Measurements. The reflectivity of the helium−neon (He−Ne) beam (632.8 nm wavelength) was measured to determine the phase transition temperatures of the bulk salt solutions.[34] These measurements were performed in a total internal reflection geometry using the SFG sample cell. Similar heating rates and equilibration time used in the SFG experiments are also used for reflectivity experiments. The changes in the reflected intensity depend on the changes in the refractive index during melting of the hydrates. By using the sapphire/brine two-layer system and the refractive indices of brine, sapphire, and hydrates, we have calculated the critical angle necessary for these measurements. When the temperature is higher than T_m, the critical angle for the liquid is very different from the crystals and we expect a sharp change in the intensity upon melting. On the basis of these

dx.doi.org/10.1021/ja5067866 | J. Am. Chem. Soc. 2014, 136, 14811−14820

calculations, we have used the incident angles with respect to the surface normal of the prism face of ~11° for 22 wt % NaCl, 30 wt % $CaCl_2$ solutions, and ~9° for 20 wt % $MgCl_2$ solution. These incident angles were chosen based on the critical angles of the $CaCl_2$ brine, NaCl hydrate, and $MgCl_2$ hydrate. The concentrations for all the solutions were around the eutectic point, to prevent formation of ice and phase separation between the ice and brine region. At eutectic concentrations, we expect a direct transition from aqueous solution to salt hydrates. A diode detector (brand, Newport; model, 820-SL-01) was used to measure the reflected intensity. We have used the bulk melting temperature of hydrate (Supporting Information, Table S2)[12] to calibrate the temperature of the SFG cell. The bulk melting temperatures were measured by monitoring the changes in the reflected intensity of the He−Ne laser beam. In addition, we have taken advantage of the sharp changes in the IR absorption spectra as a function of temperature to measure the bulk melting temperatures (Supporting Information, Figures S4−S7). Both IR and He−Ne measurements probe transition temperatures corresponding to a depth of few micrometers. A calibration curve (Supporting Information, Figure S3) was used to obtain corrected temperatures and to accurately calculate the surface transition temperatures measured using SFG.

Results and Discussion. The sketch of the phase diagram for $MgCl_2$, $CaCl_2$, and NaCl is shown in Figure 1. The eutectic concentrations and temperatures for these three salts are summarized in the caption of Figure 1. The general trend for all the three salts is similar. Upon cooling, the aqueous solution results in a phase separation of ice and brine-rich solution. As we cool further, the brine concentration will continue to increase until it reaches point C on the phase diagram (Figure 1) which is lower than the eutectic temperature because of supercooling. Further cooling will result in the crystallization of salt hydrates. Upon heating we expect the transition temperatures to reflect the thermodynamic phase boundaries shown in Figure 1. In the next section we discuss the SFG results for all three hydrates and a solution with an equal mole fraction of NaCl/$MgCl_2$ during cooling and heating cycles.

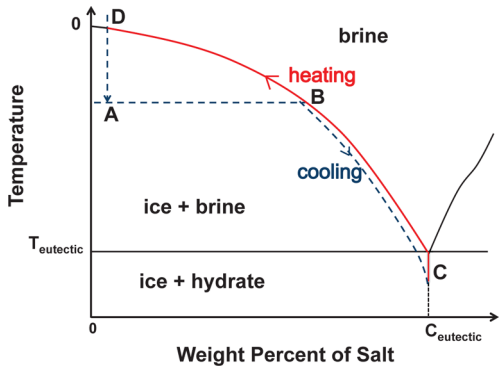

Figure 1. Phase diagram of salt solutions. When the salt solution was cooled below 0 °C, it follows the blue dashed line. When the ice forms at point A, the concentration of the brine increases from point A to point B. As the temperature is decreased further, more ice forms and the concentration of salt solution increases along this blue dashed line (indicated by the arrows) until the eutectic point is reached. The hydrate forms at point C. On heating, the path is reversed, and the hydrate melts. Finally, the ice will melt at point D which depends on the primary concentration of the salt solution. In this figure, $T_{eutectic}$ ($MgCl_2 \cdot 12H_2O$) = −33.5 °C, $C_{eutectic}$ ($MgCl_2 \cdot 12H_2O$) = 21 wt %; $T_{eutectic}$ ($CaCl_2 \cdot 6H_2O$) = −49.8 °C, $C_{eutectic}$ ($CaCl_2 \cdot 6H_2O$) = 30 wt %; $T_{eutectic}$ ($NaCl \cdot 2H_2O$) = −21.2 °C, $C_{eutectic}$ ($NaCl \cdot 2H_2O$) = 23 wt %. The original phase diagram is reconstructed from the CRC Handbook.[12]

$MgCl_2 \cdot 12H_2O$ Hydrate. Figure 2 shows the SFG spectra in PPP polarization during cooling (a) and heating (b) cycles for a low concentration (0.1 M, 0.9 wt %) $MgCl_2$ solution (the SSP data are provided in Supporting Information, Figure S1). In the aqueous solution, we observe three main peaks at ~3200, ~3450, and ~3720 cm^{-1}. The ~3720 cm^{-1} peak has been assigned to the stretching mode of the dangling OH group on the sapphire surface.[30,31,35,36] Recently it has been pointed out that the non-hydrogen bonded OH stretching vibration of water molecules could also contribute to the signal observed near ~3700 cm^{-1}.[37] The two broad peaks at ~3200 and ~3450 cm^{-1} correspond to the strong tetrahedrally coordinated hydrogen-bond stretching modes and to lower coordination hydrogen-bond stretching modes, respectively.[38,39] Compared to the SFG spectra for water/sapphire interfaces, the intensity of the ~3200 cm^{-1} peak was lower than that of the peak at ~3450 cm^{-1}, which was also observed in the SFG spectra of $MgCl_2$ solutions at the air−liquid interface in previous publications.[10,40] These differences can be explained as due to the disruption of the water−water hydrogen bonds by salt ions.[41] The increase in the ratio of the ~3450 cm^{-1} peak intensity to the ~3200 cm^{-1} peak intensity was also observed in both IR and Raman spectra of the $MgCl_2$ solution, particularly at higher concentrations.[40]

Interestingly, as we cool the system further, we observe an ice peak near ~3100 cm^{-1}, in addition to the broad hydroxyl peaks associated with water (Figure 2a). This implies that ice crystal clusters form at the sapphire surface surrounded by the concentrated brine. Upon further cooling, sharp peaks (between 3200 and 3600 cm^{-1}) are observed in addition to the ice peak (near ~3100 cm^{-1}), which indicates crystallization of $MgCl_2$ hydrate. The peak assignments for the hydrate peaks observed using SFG and from previous Raman spectra[20] are summarized in Table 1. On the basis of Raman data, we expect six peaks corresponding to the six types of OH stretching modes for a $MgCl_2 \cdot 12H_2O$ crystal unit cell.[15,17,42] We find five peaks were sufficient to obtain good fits, and the peak positions were very similar (within 7 cm^{-1}) to those reported in the Raman experiments (Table 1). We did not use the 3422 cm^{-1} peak in fitting the SFG data because that peak only appears as a weak shoulder in the Raman experiments,[20] which were also conducted at very low temperatures (−170 °C).

Figure 2b shows the changes in the SFG spectra during the heating cycle after the formation of the $MgCl_2$ hydrate. The sharpness and the intensities of the hydrate peaks reduce as we heat it toward the bulk melting temperature of the hydrate. Near −33 °C, we observe a sudden change in the SFG spectra and the hydrate peaks vanish, suggesting the melting of the $MgCl_2 \cdot 12H_2O$ hydrate. This transition temperature is similar to that reported for the melting temperature of bulk $MgCl_2 \cdot 12H_2O$ crystals (−33.5 °C). The differences in the melting and freezing temperatures (hysteresis) is provided in Supporting Information, Table S1. The values of the amplitude strength (A_q) of the major hydrate peak (3455 cm^{-1}) as a function of temperature are provided in the Supporting Information (Figure S8). The values of A_q do not change sharply. However, the sharp peaks disappear upon heating indicating that the hydrates next to the sapphire surface have melted. After the melting of the hydrate crystal, the ice peak is present, indicating the persistence of ice crystals near the sapphire substrate (Figure 2). Surprisingly, the ice peak melts at −9 °C, below the transition temperature expected based on the bulk phase diagram (~0 °C for 0.1 M, 0.9 wt % concentration solution, Figure 1). In the heating experiments, the concentration of brine should continuously decrease until it equals the starting concentration before the cooling cycle (0.1 M, 0.9 wt %). The continuous changes in concentration require melting of the ice to continuously add water to the brine layer as we heat the sample to 0 °C. The SFG data supports the hypothesis that the brine layer has segregated next to the sapphire interface[30] and is mixed with ice crystals, and that the surface ice crystals melt first to reduce the brine concentrations as we heat the sample. This is the reason we do not observe any distinctive changes in the SFG spectra as we crossed the expected bulk transition temperature near 0 °C. If we use the Gibbs−Thomson equation to calculate the depression in T_m as a function of crystal size; a depression in T_m by 9 °C corresponds to a maximum crystal size of ~13 nm (the details of the calculations are provided in Supporting Information). The crystals with higher surface area/volume ratio melt before the bulk melting temperature because of higher surface energy. It is also interesting to note that Raman data[18,20] for the $MgCl_2$ hydrate inclusions show that hydrate crystal peaks are accompanied by a strong ice peak, suggesting that $MgCl_2$ hydrate crystals are interdispersed with small ice crystals.

dx.doi.org/10.1021/ja5067866 | J. Am. Chem. Soc. 2014, 136, 14811−14820

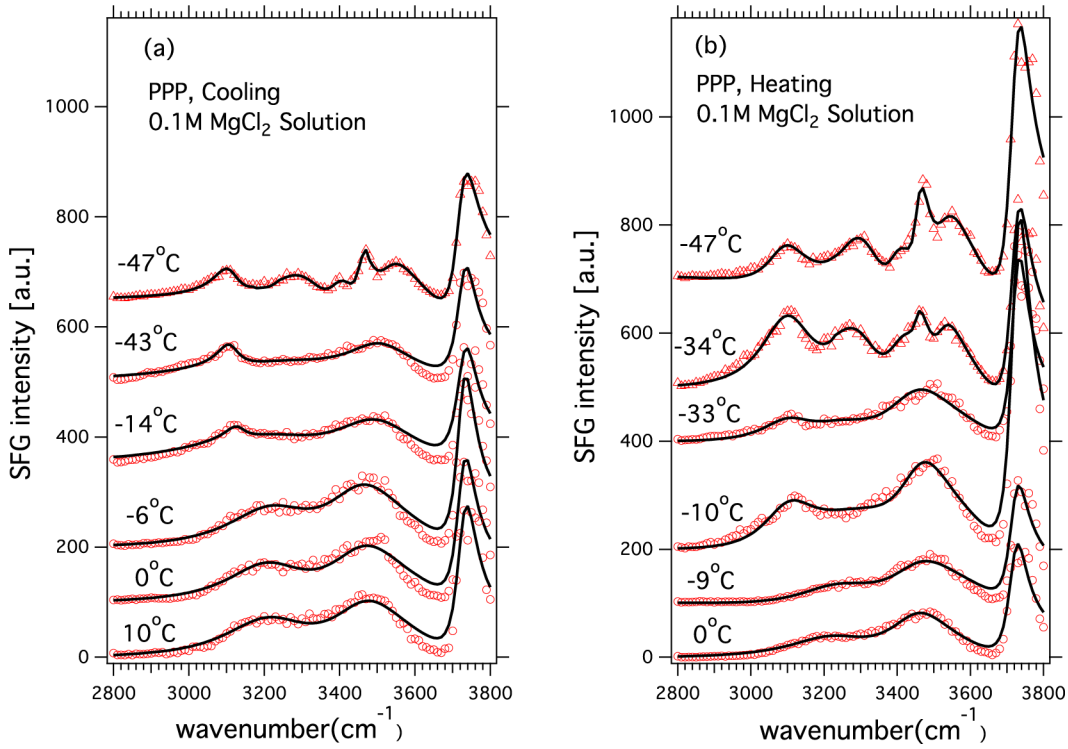

Figure 2. Formation of $MgCl_2 \cdot 12H_2O$ at low concentration. SFG spectra collected for 0.1 M (0.9 wt %) $MgCl_2$ solution in PPP polarization during cooling (a) and heating (b) cycles. The open triangles and circles correspond to temperatures where $MgCl_2 \cdot 12H_2O$ hydrate and brine are in contact with the sapphire substrate, respectively. The solid lines are the fits using the Lorentzian equation and the fitting results are summarized in the Supporting Information (Tables S3–S4). The melting temperatures for the hydrate are at −33 ± 1 °C. The ice peak disappears at −9 ± 1 °C.

Table 1. Comparison of $MgCl_2 \cdot 12H_2O$ Peak Assignments (cm^{-1}) for Raman[20] and SFG Spectroscopy

T = −47 °C	T = −36 °C	T = −170 °C
SFG(PPP) (cm^{-1})	SFG(SSP[a]) (cm^{-1})	Raman (cm^{-1})
3250	3251	3250
3322	3322	3322
3392	3404	3397
		3422
3455	3465	3458
3518	3518	3511

[a]The SFG spectra in the SSP polarization during the heating cycle are shown in Supporting Information Figure S1. The fitting parameters for the SFG spectra in SSP polarization are summarized in Supporting Information Table S5.

To explore the influence of the concentration of the starting solution, we also performed the SFG experiments with highly concentrated (20 wt %) $MgCl_2$ solution, shown in Figure 3a. Comparing Figure 2 to Figure 3a, we observe that the 3200 cm^{-1} peak is much weaker for high $MgCl_2$ concentrations. Additionally, there are differences in the SFG spectra collected using low concentration salt solution and then cooling it toward the eutectic concentration, compared to the solutions we started with the concentrations similar to the eutectic concentration. We also observe a strong peak at 3600 cm^{-1}, and the large variability in the magnitude and the type of surface hydroxy groups could be due to a range of isoelectric points reported for these sapphire prisms as reported in our earlier studies.[44] The hydrate structure is also not identical to the one shown in Figure 2, and the ratio of these six hydrate peaks are different. We anticipate that the crystal orientation may play a big role in changing the ratio of these hydrate peaks.[19,20,24] We also do not observe a strong ice peak in the SFG spectra in Figure 3a. It is important to note that the weight percentage of $MgCl_2$ salt to the $MgCl_2 \cdot 12H_2O$ hydrate is around 31 wt %. For the 20 wt % $MgCl_2$ solution, it should directly form a mixture of hydrate and ice. However, only clear $MgCl_2$ hydrate peaks are observed, consistent with the conclusion that hydrate crystallizes next to sapphire surfaces.

To compare the differences between the surface and bulk melting temperatures for the $MgCl_2$ hydrates next to a solid surface, we measured the intensity of the reflected He–Ne light for the 20 wt % $MgCl_2$ solution. Figure 3b shows a sharp change in the reflected intensity between −34 and −33 °C for the $MgCl_2 \cdot 12H_2O$. Similar conclusions are reached by monitoring the IR absorption in total internal reflection geometry (Supporting Information: Figure S4). These measurements indicate that the surface transition temperatures are similar to the bulk transition temperatures for the $MgCl_2 \cdot 12H_2O$ hydrate.

$CaCl_2 \cdot 6H_2O$ Hydrates. Figure 4a shows selected SFG spectra collected in PPP polarization during the cooling cycle of 0.1 M (1 wt %) $CaCl_2$ solution (the SSP spectrum is provided in Supporting Information, Figure S2). The relative SFG intensity for the ∼3450 cm^{-1} peak is higher than the ∼3200 cm^{-1} peak in the liquid brine solution. In addition, the ∼3100 cm^{-1} ice peak is present together with brine peaks at low temperature. Upon cooling further, we observe one sharp SFG peak at 3426 cm^{-1}, and three weaker hydrate peaks (Figure 4a). We also observe an ice peak at 3135 cm^{-1}, in addition to the four hydrate peaks. The peak position for the major hydrate peak is similar to that observed using Raman spectroscopy,[18,20,45] and this indicates the formation of a $CaCl_2$ hydrate unit cell with six water molecules ($CaCl_2 \cdot 6H_2O$ hydrate, Table 2). There are small differences in the location of the shoulder peaks observed in the SFG spectra in comparison to Raman results. In addition to the factors discussed for $MgCl_2$ hydrates, the reasons for these difference of $CaCl_2$ hydrate could be due to the very weak shoulder peaks overlapping with the broad and dominating SFG peak at 3426 cm^{-1}. Also, for $CaCl_2$ hydrate, there is an additional contribution to the SFG signals due to the SFG signals from the bulk, because $CaCl_2 \cdot 6H_2O$ forms a noncentrosymmetric crystal (space group $P321$, crystal class 32)[14] and this could also influence the dominance of some peaks over the others. However, the dominant peak is similar to that measured by Raman spectroscopy. In comparison, the space groups for $NaCl \cdot 2H_2O$[16] and $MgCl_2 \cdot 12H_2O$[15] are $P2_1/n$, which are centrosymmetric, so

dx.doi.org/10.1021/ja5067866 | J. Am. Chem. Soc. 2014, 136, 14811–14820

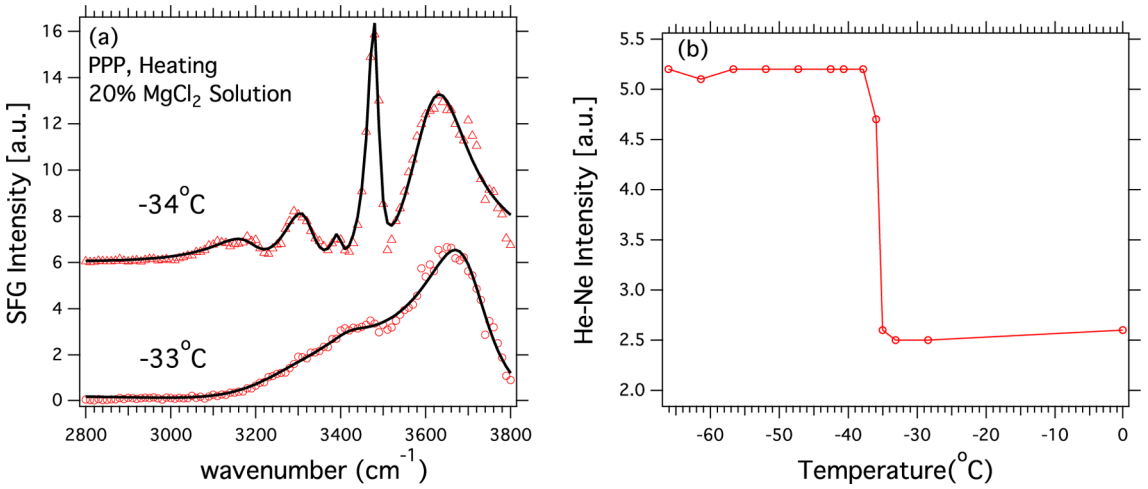

Figure 3. Formation of $MgCl_2 \cdot 12H_2O$ at high concentration. (a) SFG spectra collected for 20 wt % $MgCl_2$ solution in PPP polarization during heating cycles. The open triangles and circles correspond to temperatures at which the $MgCl_2 \cdot 12H_2O$ hydrate and brine are in contact with the sapphire substrate, respectively. The solid lines are the fits using the Lorentzian equation and the fitting results are summarized in the Supporting Information (Table S6). The melting temperatures for the hydrate are at -33 ± 1 °C. (b) Scan of He−Ne reflected intensity vs temperature for 20 wt % $MgCl_2$ solution next to sapphire substrate in a heating cycle.

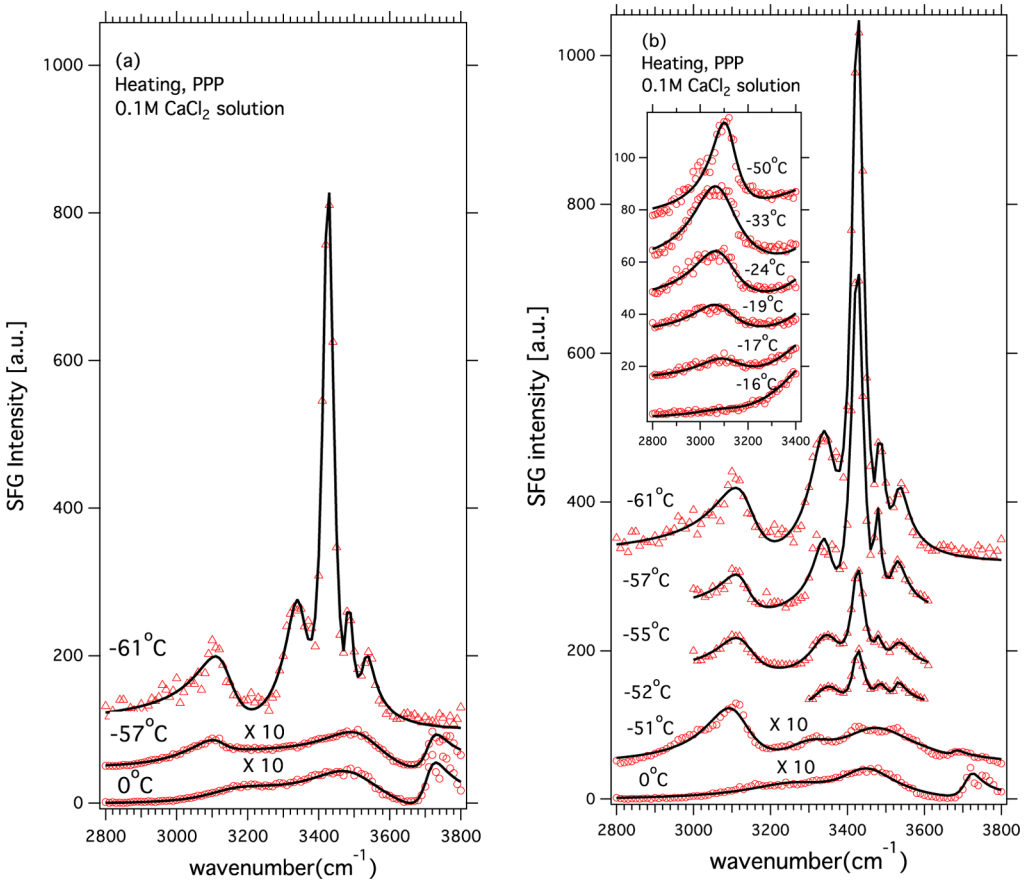

Figure 4. Formation of $CaCl_2 \cdot 6H_2O$ at low concentration. SFG spectra collected for 0.1 M (1 wt %) $CaCl_2$ solution in PPP polarization during cooling (a) and heating (b) cycles. The empty triangles and circles correspond to temperatures where $CaCl_2 \cdot 6H_2O$ hydrate and brine are in contact with the sapphire substrate, respectively. The solid lines are the fits using the Lorentzian equation; the fitting results are summarized in the Supporting Information (Tables S7−S8). The melting temperature for the hydrate is -50 ± 1 °C. The ice peak information is provided as the inset of the figure, and the ice peak disappears at -16 ± 1 °C.

we do not expect the bulk to contribute to the SFG signals in these two crystals.

Figure 4b shows selected SFG spectra during the heating cycle after the formation of the $CaCl_2$ hydrates. The values of A_q for the 3426 cm^{-1} peak as a function of temperature are provided in the Supporting Information (Figure S9). The values of A_q continue to decrease in the heating cycle, and near −51 °C we observe a sharp change in the magnitude of A_q. The gradual decrease in A_q before the melting

dx.doi.org/10.1021/ja5067866 | J. Am. Chem. Soc. 2014, 136, 14811−14820

Table 2. Comparison of $CaCl_2·6H_2O$ Peak Assignments for Raman[18] and SFG Spectroscopy

T = −61 °C		T = −170 °C
SFG(PPP) (cm^{-1})	SFG(SSP[a]) (cm^{-1})	Raman (cm^{-1})
	3281	3242
3347		3384
		3407
3426	3420	3433
3482	3491	3513
3529		

[a]The SFG spectrum for $CaCl_2·6H_2O$ in SSP polarization at −61 °C is shown in Supporting Information, Figure S2. The fitting parameters for the SFG spectra in SSP polarization are summarized in Supporting Information, Table S9.

temperature could indicate partial melting of the hydrate structure or softening[43] of the crystal structure before the complete disappearance of the hydrate peaks above T_m. The changes in the reflected intensity measured using the He−Ne laser and the IR absorption experiments (Supporting Information Figure S5) drops near −49 °C. The differences in the melting and freezing temperatures (hysteresis) is provided in Supporting Information, Table S1. After the melting of the hydrate crystals, we continue to observe an ice peak similar to that observed for the $MgCl_2$ hydrates (inset of Figure 4b), and this ice peak disappears at −16 ± 1 °C. This depression of melting temperature corresponds to a maximum crystal size of ∼7 nm (calculated by Gibbs−Thomson eq (Supporting Information, section 2). These smaller crystals melted before the bulk ice layer due to their higher surface area/volume ratio and excess surface energy. Figure 5a shows the SFG spectra for 30 wt % $CaCl_2$ solution (close to the eutectic concentration) during the heating cycle. Interestingly, the hydrate peak at 3426 cm^{-1} is more intense than either the water or the ice peak, owing to a higher contribution from the $CaCl_2·6H_2O$ hydrate signal from the bulk. The hydrate signals for high concentrations are higher than that for lower concentration because of a much more uniform and ordered crystal layer near the sapphire interface.

NaCl·2H$_2$O Hydrate. The results for the low concentration NaCl hydrate were presented in an earlier publication.[30] Here we show the results from the heating cycle for high concentration (22 wt %, near eutectic concentration) NaCl solution (Figure 6a). Similar to the low concentration results, we observe one strong peak at 3416 cm^{-1} and a smaller peak at 3540 cm^{-1}. The relative ratios of these two peaks are different from those collected for low concentrations. No ice peak was observed for NaCl solutions, indicating that a brine layer has segregated next to the sapphire surface and has formed a uniform hydrate layer without ice. Upon heating, similar to other salts, the intensity of the hydrate peaks reduces upon heating and then vanishes abruptly near −19 ± 1 °C, indicating melting of the NaCl hydrate. The values of A_q for the ∼3416 cm^{-1} peak are shown in the Supporting Information (Figure S10). After a gradual drop in the values of A_q we observed a sharp change in A_q near −20 °C. These results suggest that the surface and the bulk structures of NaCl hydrates at the transition temperatures are very similar to each other.

NaCl−MgCl$_2$−H$_2$O Mixture. The hydrate results indicate that the NaCl hydrate forms a uniform layer next to the surface, while the $MgCl_2$ and $CaCl_2$ hydrates are mixed with ice at the surface. Next, we discuss the cooling and heating experiments on equal molarities of NaCl and $MgCl_2$ solutions to determine whether there is a tendency for one or both hydrates to form next to the sapphire substrate. From the ternary phase diagram of the NaCl−$MgCl_2$−H_2O system,[46,47] we expect the solution to form a mixture of ice, NaCl·2H_2O, and $MgCl_2·12H_2O$ in the bulk. On the basis of the ternary phase diagram (Supporting Information Figure S12), the $MgCl_2$ hydrates are expected to melt at −35 °C (point A in Figure S12). Further heating will result in melting of the NaCl hydrates gradually as we go from point A to point B in Figure S12. This will increase the concentration of NaCl in the brine and also decrease the concentration of the $MgCl_2$ in the brine phase. Between the eutectic temperature −35 °C and −21.2 °C, all the NaCl hydrate crystals are expected to melt. The transition temperature of NaCl hydrates will depend on the concentration of the salt solution.

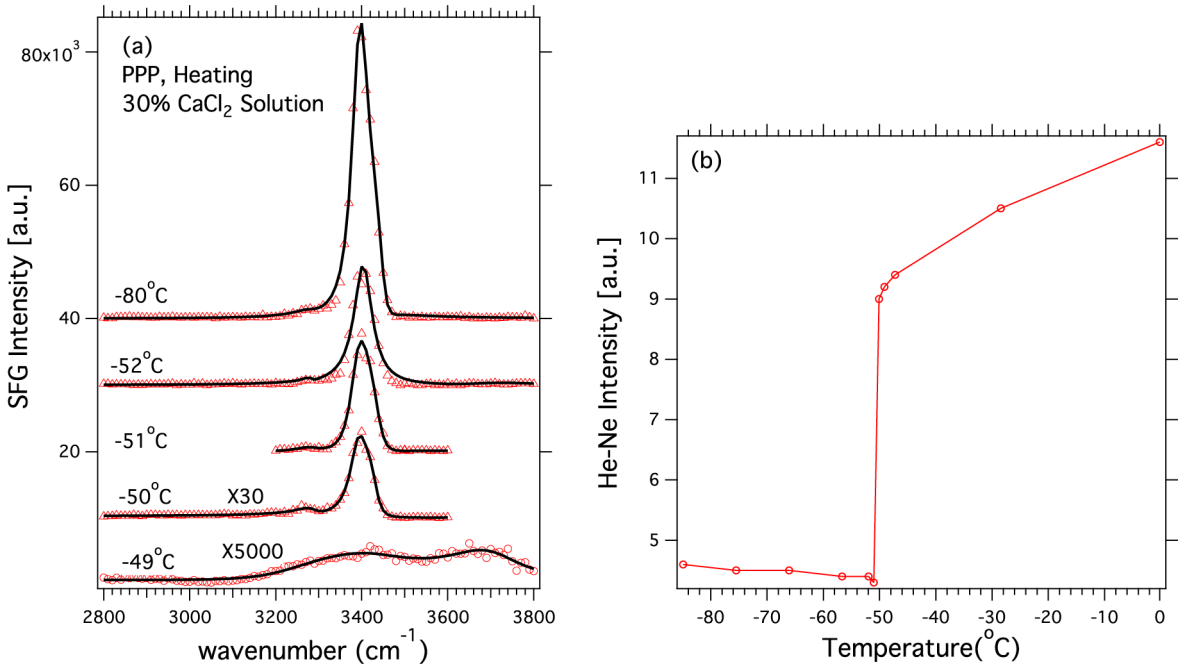

Figure 5. Formation of $CaCl_2·6H_2O$ at high concentration. (a) SFG spectra collected for 30 wt % $CaCl_2$ solution in PPP polarization during heating cycles. The empty triangles and circles correspond to temperatures at which $CaCl_2·6H_2O$ hydrate and brine are in contact with the sapphire substrate, respectively. The solid lines are the fits using the Lorentzian equation and the fitting results are summarized in the Supporting Information (Table S10). The melting temperatures for the hydrate are at −49 ± 1 °C. (b) Scan of He−Ne reflected intensity vs temperature for 30 wt % $CaCl_2$ solution next to sapphire substrate in a heating cycle.

dx.doi.org/10.1021/ja5067866 | J. Am. Chem. Soc. 2014, 136, 14811−14820

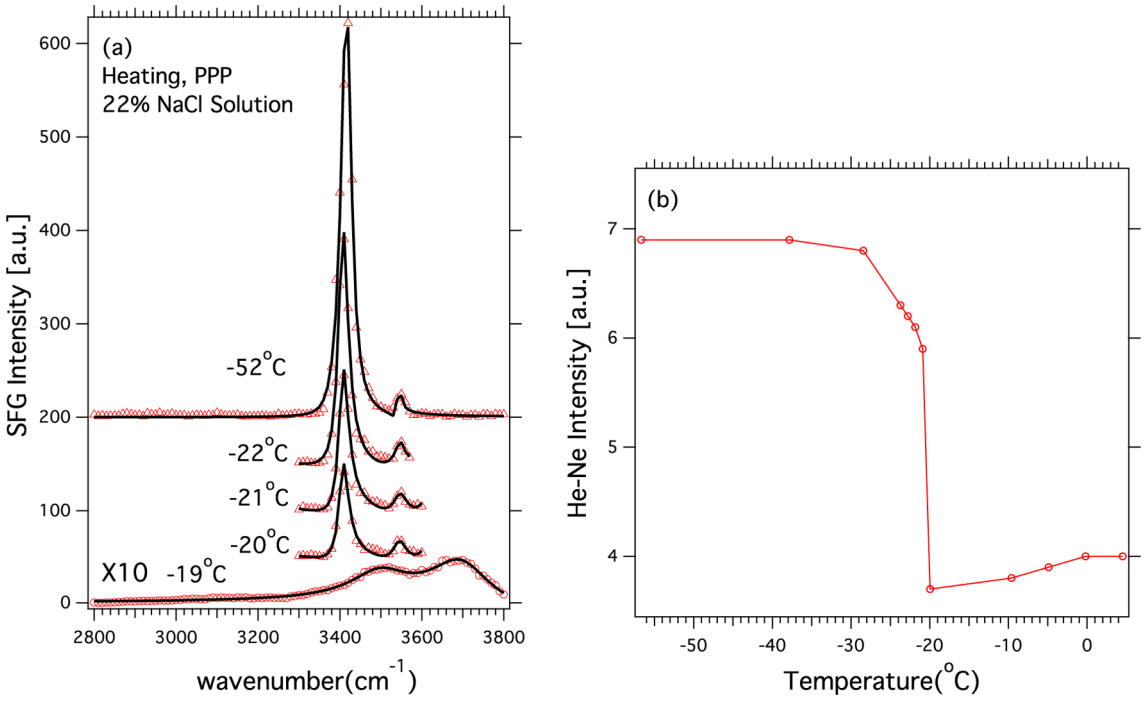

Figure 6. Formation of $NaCl{\cdot}2H_2O$ at high concentration. (a) SFG spectra collected for 22 wt % NaCl solution in PPP polarization during heating cycles. The empty triangles and circles correspond to temperatures at which $NaCl{\cdot}2H_2O$ hydrate and brine are in contact with the sapphire substrate, respectively. The solid lines are the fits using the Lorentzian equation, and the fitting results are summarized in the Supporting Information Table S11. The melting temperature for the hydrate is -19 ± 1 °C. (b) Scan of He−Ne reflected intensity vs temperature for 22 wt % $NaCl_2$ solution next to sapphire substrate in a heating cycle.

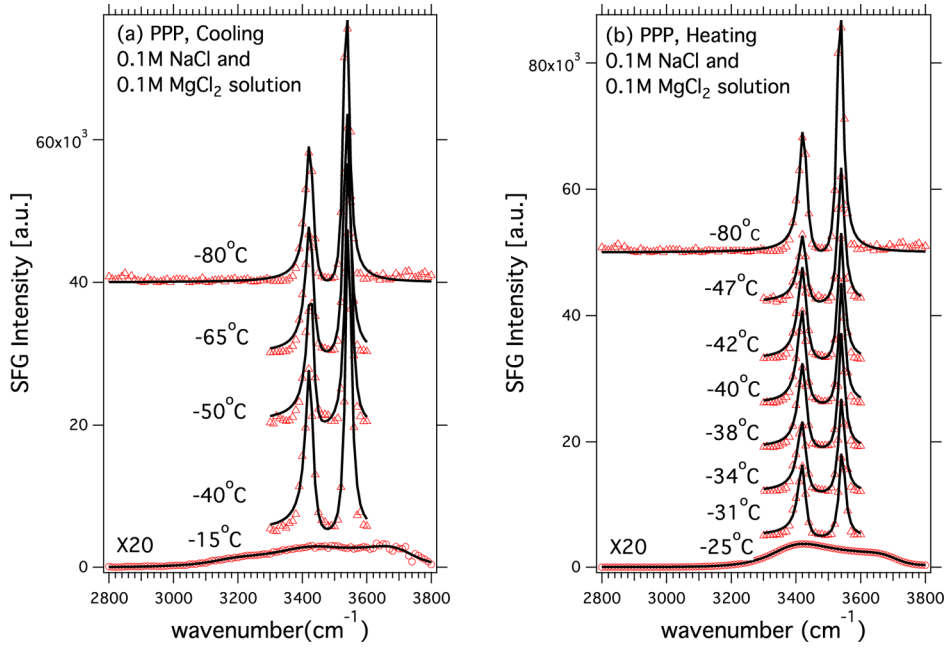

Figure 7. Formation of hydrates from the mixed solution. SFG spectra collected for 0.1 M (0.6 wt %) NaCl and 0.1 M (0.9 wt %) $MgCl_2$ mixture solution in PPP polarization during cooling (a) and heating (b) cycles. The empty triangles and circles correspond to temperatures where hydrate and brine are in contact with the sapphire substrate, respectively. The solid lines are the fits using the Lorentzian equation, and the fitting results are summarized in the Supporting Information Tables S12−S13. The melting temperatures for the hydrate are at -25 ± 1 °C.

Figure 7a shows selected SFG spectra in PPP polarization during cooling cycles for a low concentration of an aqueous solution containing 0.1 M (0.6 wt %) NaCl and 0.1 M (0.9 wt %) $MgCl_2$. The brine spectra show a higher ~3450 cm^{-1} peak than the ~3200 cm^{-1} peak, which is similar to the brine spectra of $MgCl_2$ solution. However, upon cooling, we do not observe a peak at ~3100 cm^{-1} corresponding to the ice peak, which is similar to the results obtained for the brine spectra of NaCl solution. By cooling at a rate of 1 °C/min with 10 min equilibrium time between every degree change in temperature, we observe two sharp high intensity SFG peaks (at 3420 and 3540 cm^{-1}) near −40 °C (Figure 7a). The peak positions for the two peaks are the same as those observed for $NaCl{\cdot}2H_2O$ in SFG, IR, and Raman spectroscopy, which indicate the

dx.doi.org/10.1021/ja5067866 | J. Am. Chem. Soc. 2014, 136, 14811−14820

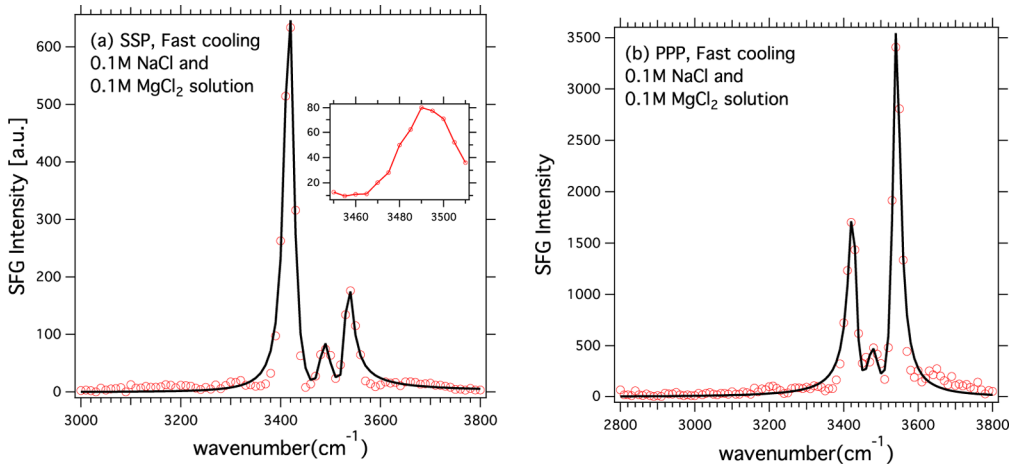

Figure 8. SFG spectra collected for the hydrates formed from 0.1 M NaCl and 0.1 M $MgCl_2$ mixed solution for SSP (a) and PPP (b) polarization in the fast cooling cycle, at a rate (5 °C/min) with 5 min equilibrium time every 10 °C. The inset is the SFG spectra in the range from 3450 to 3510 cm^{-1} with a scanning step size of 5 cm^{-1}. The open circles correspond to SFG intensity of the mixture of $NaCl{\cdot}2H_2O$ and $MgCl_2{\cdot}12H_2O$ hydrates in contact with the sapphire substrate. The solid lines are the fits using the Lorentzian equation, and the fitting results are summarized in the Supporting Information (Table S14).

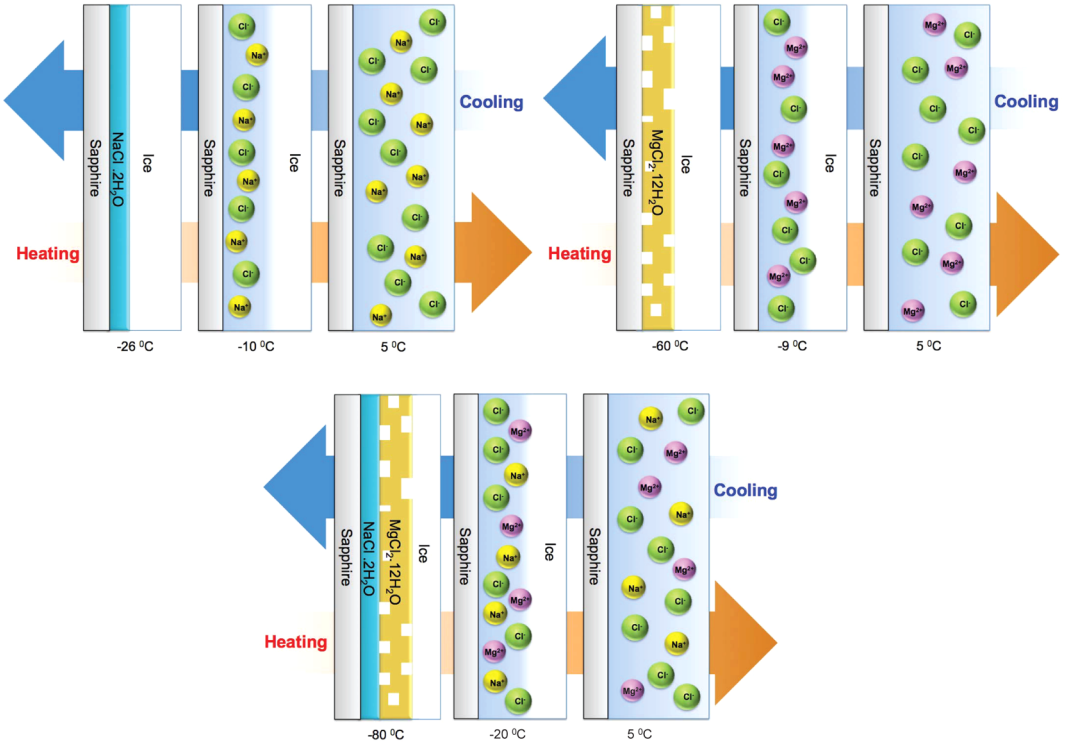

Figure 9. Illustration for surface segregation and hydrate crystals formation for the three salt solutions (0.1 M $MgCl_2$, 0.1 M NaCl, and their mixtures). In cooling, the brine-rich layers segregate to the sapphire surface. NaCl solution forms a uniform hydrate layer without ice. The $MgCl_2$ solution forms a hydrate layer mixed with ice. The NaCl and $MgCl_2$ mixed solution forms a uniform NaCl hydrate layer without ice or $MgCl_2$ hydrate at the sapphire surface. We have illustrated in this model the boundaries between the ice and brine/hydrate phases to be sharp, and it is not necessary that these boundaries are flat.

formation of $NaCl{\cdot}2H_2O$ at the sapphire surface. Interestingly, the intensity ratio of the two peaks observed for the mixture is different from the $NaCl{\cdot}2H_2O$ hydrate intensity ratio in the NaCl solution, which suggests differences in the orientation of the hydrate crystals,[20] formed from the NaCl-$MgCl_2$ solution and a single component NaCl solution next to the sapphire surface. When we cool the system further down to −80 °C, the spectra remain the same and we do not observe $MgCl_2$ hydrate peaks in the SFG spectra. The intensity of the NaCl hydrate peaks observed in the SFG spectra for the mixture and the NaCl solution are comparable, which indicates that a uniform layer of the NaCl hydrate has formed next to the sapphire surface.

Figure 7b shows the SFG spectra during the heating cycle after the formation of the salt hydrates. The intensity of both peaks decreases slightly, and the intensities of two NaCl hydrate peaks become more comparable upon heating. We observe a gradual decrease in SFG intensity of the NaCl hydrate and then a much sharper decrease in the A_q of the NaCl hydrate peak at −25 °C (Supporting Information Figure S11). The sharp drop in A_q at −25 °C suggests that melting of the NaCl hydrates proceeds from the bulk and then finally the surface. Interestingly, the melting of the salt hydrates is at a slightly lower temperature than that expected from the pure NaCl phase diagram (−21 °C) due to the influence of the $MgCl_2$ brine phase.

dx.doi.org/10.1021/ja5067866 | J. Am. Chem. Soc. 2014, 136, 14811−14820

When the NaCl and $MgCl_2$ solution is cooled at a faster rate (5 °C/min) with 5 min equilibrium time every 10 °C, peaks belonging to $NaCl{\cdot}2H_2O$ and $MgCl_2{\cdot}12H_2O$ are observed (Figure 8), suggesting that if the time is not sufficient for equilibration, the hydrate formation is not uniform, and that the $MgCl_2{\cdot}12H_2O$ hydrates may also form (together with the NaCl hydrates) next to the sapphire surface. The IR absorption experiment (Supporting Information Figure S7) for the mixture shows both NaCl and $MgCl_2$ hydrate peaks, consistent with the ternary phase diagram for this system and the SFG results.[46,47]

The experimental results are summarized in the diagram shown in Figure 9. For all three salt solutions (NaCl, $MgCl_2$, and $CaCl_2$), we observe that the brine solution segregates next to the sapphire substrate. For NaCl we did not observe any surface ice crystals near the sapphire substrate. In addition, we are unable to discern an ice peak in the IR spectra reported in the SI (Figure S6). Therefore, formation of a NaCl brine (and hydrate) phase next to the sapphire and an ice phase away from the surface is supported by the experimental observations. The model for $MgCl_2$ is built on the observations of surface ice crystals observed in the SFG experiment. Although we do not directly observe an ice layer away from the surface, we do know from the phase diagram that there must be an ice layer which should melt near 0 °C for the 0.1 M $MgCl_2$ solution. Since it is not observed near the surface, we are only left with the possibility that it has to be away from the surface. A similar argument can be made for the mixture of $MgCl_2$ and NaCl. In the slow cooling conditions, we have not observed the $MgCl_2$ hydrates next to the surface, and this supports the idea that the NaCl hydrate has to be near the sapphire substrate.

SUMMARY

In summary, the results of Mg, Ca, and Na-hydrate formation near surfaces indicate striking similarities and differences. The brine-rich layer segregates next to the sapphire surface upon cooling. For $MgCl_2$ and $CaCl_2$, the brine-rich layer has ice-crystals mixed with the brine layer. For NaCl the brine layer is more uniform and no ice crystals were observed. For the NaCl-$MgCl_2$ salt mixture, the brine-rich layer forms a uniform NaCl hydrate layer without any ice crystals or $MgCl_2$ hydrate crystals next to the sapphire surface (Figure 9). The signals for $CaCl_2{\cdot}6H_2O$ at high concentrations are due to the combination of surface and bulk contributions, because the $CaCl_2$–hydrate forms noncentrosymmetric crystals. The positions of the major hydrate peaks in all three cases match with those reported using Raman spectroscopy, and the surface and bulk crystals are similar. The relative intensity of the hydrate peaks varies, depending on the orientation of the hydrate crystals. Interestingly, we also observe sharp hydrate peaks at temperatures where the bulk hydrate peaks are much broader, indicating that more uniform crystals are formed next to the sapphire substrate. The intensity of the hydrate peaks drops slowly before the actual melting temperature, indicating a softening of the crystal structure before melting. Similar softening of the crystal structure has been observed for ice melting at the air–ice interface[48] and melting of salt hydrates.[18] The main melting transition temperatures for the hydrates at the surface are very similar to those of the bulk hydrates. Surprisingly, the surface ice crystals observed for the $MgCl_2$ and $CaCl_2$ solutions melt at much lower temperature than that expected from the phase diagram due to higher surface/volume ratio and excess surface energy for these nanometer-size surface crystals. This study highlights the role of surfaces in controlling the segregation of brine and salt hydrates and raises an important future question on how different mineral and rock surfaces may influence the formation of ice and salt hydrates.

ASSOCIATED CONTENT

Supporting Information

Hysteresis table; phase diagram of NaCl–$MgCl_2$–H_2O system, SSP spectra, experimental setup, IR spectra and results of fits. This material is available free of charge via the Internet at http://pubs.acs.org.

AUTHOR INFORMATION

Corresponding Author

ali4@uakron.edu

Notes

The authors declare no competing financial interest.

ACKNOWLEDGMENTS

The authors thank Edward Laughlin, Anish Kurian, and Liehui Ge for their help in designing the temperature stage. We also thank He Zhu, Mena Klittich, and Nishad Dhopatkar for helpful discussion. We are grateful for the financial support from the National Science Foundation.

REFERENCES

(1) Zalba, B.; Marín, J. M.; Cabeza, L. F.; Mehling, H. *Appl. Therm. Eng.* **2003**, *23*, 251–283.
(2) Sharma, A.; Tyagi, V. V.; Chen, C. R.; Buddhi, D. *Renew. Sust. Energy Rev.* **2009**, *13*, 318–345.
(3) Wang, Y.; Von Euw, S.; Fernandes, F. M.; Cassaignon, S.; Selmane, M.; Laurent, G.; Pehau-Arnaudet, G.; Coelho, C.; Bonhomme-Coury, L.; Giraud-Guille, M.-M.; Babonneau, F.; Azas, T.; Nassif, N. *Nat. Mater.* **2013**, *12*, 1144–1153.
(4) Glimcher, M. J. *Rev. Mineral. Geochem.* **2006**, *64*, 223–282.
(5) Worsnop, D. R.; Zahniser, M. S.; Fox, L. E.; Wofsy, S. C. *Science* **1993**, *259*, 71–74.
(6) Vaniman, D. T.; Bish, D. L.; Chipera, S. J.; Fialips, C. I.; Carey, J. W.; Feldman, W. C. *Nature* **2004**, *431*, 663–665.
(7) Peterson, R. C.; Wang, R. *Geology* **2006**, *34*, 957–960.
(8) Hennings, E.; Heinz, J.; Schmidt, H.; Voigt, W. *Z. Anorg. Allg. Chem.* **2013**, *639*, 922–927.
(9) Escamilla-Roa, E.; Sainz-Díaz, C. I. *J. Phys. Chem. C* **2014**, *118*, 3554–3563.
(10) Casillas-Ituarte, N. N.; Callahan, K. M.; Tang, C. Y.; Chen, X.; Roeselová, M.; Tobias, D. J.; Allen, H. C. *Proc. Natl. Acad. Sci. U.S.A.* **2010**, *107*, 6616–6621.
(11) Roedder, E. *Rev. Mineral.* **1984**, *12*, 1–664.
(12) Lide, D. R., Ed. *CRC Handbook of Chemistry and Physics*, 86th ed.; CRC Press: Boca Raton, FL, 2005.
(13) Weck, P. F.; Kim, E. *J. Phys. Chem. C* **2014**, *118*, 4618–4625.
(14) Torii, T.; Ossaka, J. *Science* **1965**, *149*, 975–977.
(15) Sasvari, K.; Jeffrey, G. *Acta Crystallogr.* **1966**, *20*, 875–881.
(16) Klewe, B.; Pedersen, B. *Acta Crystallogr., Sect. B: Struct. Sci.* **1974**, *30*, 2363–2371.
(17) Hennings, E.; Schmidt, H.; Voigt, W. *Acta Crystallogr., Sect. C: Cryst. Struct. Commun.* **2013**, *69*, 1292–1300.
(18) Dubessy, J.; Audeoud, D.; Wilkins, R.; Kosztolanyi, C. *Chem. Geol.* **1982**, *37*, 137–150.
(19) Bakker, R. J. *Can. Mineral.* **2004**, *42*, 1283–1314.
(20) Baumgartner, M.; Bakker, R. J. *Chem. Geol.* **2010**, *275*, 58–66.
(21) Hester, R. E.; Krishnan, K.; Scaife, C. W. J. *J. Chem. Phys.* **1968**, *49*, 1100–1110.
(22) Franks, F. *Water: A Comprehensive Treatise. Vol. 1. The Physics and Physical Chemistry of Water*; Plenum Publishing Corporation: New York, 1972.
(23) Lucchesi, P. J.; Glasson, W. A. *J. Am. Chem. Soc.* **1956**, *78*, 1347–1348.
(24) Lutz, H. *Bonding and Structure of Water Molecules in Solid Hydrates. Correlation of Spectroscopic and Structural Data*; Springer: New York, 1988; pp 97–125.
(25) Miyata, K.; Kanno, H.; Niino, T.; Tomizawa, K. *Chem. Phys. Lett.* **2002**, *354*, 51–55.
(26) Saunders, R. W.; Möhler, O.; Schnaiter, M.; Benz, S.; Wagner, R.; Saathoff, H.; Connolly, P.; J; Burgess, R.; Gallagher, M.; Will, R.; Murray, B. J.; Plane, J. M. C. *Atmos. Chem. Phys.* **2010**, *10*, 1227–1247.

(27) Atkinson, J. D.; Murray, B. J.; Woodhouse, M. T.; Whale, T. F.; Baustian, K. J.; Carslaw, K. S.; O'Sullivan, D.; Malkin, T. L. *Nature* **2013**, *498*, 355−358.
(28) Paterson, W. *The Physics of Glaciers*; Butterworth-Heinemann: Oxford, UK, 1994.
(29) McCord, T. B.; Hansen, G. B.; Hibbitts, C. A. *Science* **2001**, *292*, 1523−1525.
(30) Anim-Danso, E.; Zhang, Y.; Dhinojwala, A. *J. Am. Chem. Soc.* **2013**, *135*, 8496−8499.
(31) Anim-Danso, E.; Zhang, Y.; Alizadeh, A.; Dhinojwala, A. *J. Am. Chem. Soc.* **2013**, *135*, 2734−2740.
(32) Lobau, J.; Wolfrum, K. *J. Opt. Soc. Am., B* **1997**, *14*, 2505−2512.
(33) Gautam, K.; Schwab, A.; Dhinojwala, A.; Zhang, D.; Dougal, S.; Yeganeh, M. *Phys. Rev. Lett.* **2000**, *85*, 3854.
(34) Nanjundiah, K.; Dhinojwala, A. *Langmuir* **2013**, *29*, 12168−12175.
(35) Zhang, L.; Tian, C.; Waychunas, G. A.; Shen, Y. R. *J. Am. Chem. Soc.* **2008**, *130*, 7686−7694.
(36) Sung, J.; Shen, Y. R.; Waychunas, G. A. *J. Phys.: Condens. Matter* **2012**, *24*, 124101.
(37) Boulesbaa, A.; Borguet, E. *J. Phys. Chem. Lett.* **2014**, *5*, 528−533.
(38) Du, Q.; Freysz, E.; Shen, Y. R. *Phys. Rev. Lett.* **1994**, *72*, 238−241.
(39) Shen, Y. R.; Ostroverkhov, V. *Chem. Rev.* **2006**, *106*, 1140−1154.
(40) Allen, H. C.; Casillas-Ituarte, N. N.; Sierra-Hernandez, M. R.; Chen, X.; Tang, C. Y. *Phys. Chem. Chem. Phys.* **2009**, *11*, 5538−5549.
(41) Callahan, K. M.; Casillas-Ituarte, N. N.; Xu, M.; Roeselová, M.; Allen, H. C.; Tobias, D. J. *J. Phys. Chem. A* **2010**, *114*, 8359−8368.
(42) Falk, M.; Knop, O. *Water in Crystalline Hydrates Aqueous Solutions of Simple Nonelectrolytes*; Springer: New York, 1973; pp 55−113.
(43) Lindemann, F. A. *Phys. Z.* **1910**, *11*, 609−612.
(44) Hsu, P. Y.; Dhinojwala, A. *Langmuir* **2012**, *28*, 2567−2573.
(45) Baumgartner, M.; Bakker, R. J. *Chem. Geol.* **2009**, *265*, 335−344.
(46) Dubois, M.; Marignac, C. *Econ. Geol.* **1997**, *92*, 114−119.
(47) Bakker, R. J.; Baumgartner, M. *Centr. Eur. J. Geosci.* **2012**, *4*, 225−237.
(48) Wei, X.; Miranda, P. B.; Shen, Y. *Phys. Rev. Lett.* **2001**, *86*, 1554−1557.